Check for updates

Highly-selective and sensitive plasmon-enhanced fluorescence sensor of aflatoxins†

Tetyana Sergeyeva, [ID] *[a] Daria Yarynka, [ID] [a] Vitaly Lytvyn,[b] Petro Demydov,[b] Andriy Lopatynskyi, [ID] [b,c] Yevgeny Stepanenko,[a] Oleksandr Brovko,[d] Anatoly Pinchuk[e] and Volodymyr Chegel*[b,c]

We demonstrate a novel sensor platform with enhanced sensitivity and selectivity for detecting aflatoxin B1 – a common food toxin in cereals. The approach is based on a molecularly imprinted polymer film that provides selective binding of the aflatoxin B1 and fluorescence signal from the analyte molecule enhanced by the local electric field induced in close proximity to the surface of a silver nanoparticle excited at the localized surface plasmon resonance (LSPR) wavelength. Molecularly imprinted polymers (MIPs) with supramolecular aflatoxin-selective receptor sites and embedded spherical silver nanoparticles (with diameters 30–70 nm, the LSPR band 407 nm) were prepared in the form of a thin polymer film on the surface of a glass slide using *in situ* polymerization. The detection limit of the sensor for aflatoxin B1 is 0.3 ng mL^{-1}, which is significantly lower than for a fluorescent sensor without silver nanoparticles. The plasmon-enhanced fluorescence factor is 33, and the linear dynamic range of the sensor is 0.3–25 ng mL^{-1}.

1. Introduction

Aflatoxin B1 (AFB1) is one of the most toxic substances produced by *Aspergillus* molds, contaminating various food products and feeding stuffs. Aflatoxin B1 contamination results in devastating economic burdens around the world.[1] There is an urgent need to develop a novel, low-cost, portable, and easy-to-use detection platform for fast and reliable in-field detection of aflatoxin B1 contamination. Fluorescence-based detection is one of the most promising platforms in biosensor technology, providing rapid and sensitive detection of mycotoxins. Many fluorescent sensors based on natural enzymes and receptors have been recently developed.[5–7] Aflatoxins exhibit a strong natural fluorescence signal that can be used to develop novel fluorescent sensors with enhanced selectivity and sensitivity. The fluorescence signal might help to overcome some significant limitations of the existing traditional instrumental[2,3] and immunochemical[4] analytical

methods, such as bulky and expensive equipment and long sample preparation and analysis time.[2–4] The application of nanomaterials has also attracted great interest in the biosensor domain because of their unique optical and electronic properties. For instance, noble metal nanoparticles can modify the spontaneous emission of nearby fluorescent molecules and improve the limit of detection of the analyte of interest.[8,9]

Metal nanoparticles can increase the quantum yield and improve the photostability of the analyte fluorophore molecules at optimized distances around 5–90 nm.[10–12] This phenomenon is commonly referred to as metal-enhanced fluorescence (MEF) or plasmon-enhanced fluorescence (PEF).[13,14] A few physical–chemical mechanisms are suggested to be responsible for the metal-enhanced fluorescence. First, the nanoparticle's highly enhanced local electrical field at the wavelength of localized surface plasmon resonance (LSPR) results in modified optical characteristics of the nearby fluorophore when overlapping LSPR and fluorescence spectra is provided. Specifically, metal nanoparticles act as antennas for the fluorophore, which typically results in higher emission intensity.[11,12] The shape and size of the metal nanostructures are critical for metal-enhanced fluorescence. Second, the non-radiative energy transfer between the metal nanoparticle and the fluorophore that depends on spectral overlap between the metal surface and the fluorophore plays a crucial role in fluorescence enhancement. This process is explained by Förster resonance energy transfer (FRET).[15]

The plasmon-enhanced fluorescence is widely used to increase the sensitivity of fluorescent sensors.[16,17] Typically, PEF provides ten to hundreds of enhancement factors and

[a]*Institute of Molecular Biology and Genetics, National Academy of Sciences of Ukraine, 150, Zabolotnogo Str., 03143 Kyiv, Ukraine. E-mail: t_sergeyeva@yahoo.co.uk*

[b]*V.E. Lashkaryov Institute of Semiconductor Physics, National Academy of Sciences of Ukraine, 41, prospect Nauky, 03680 Kyiv, Ukraine. E-mail: vche111@yahoo.com*

[c]*Institute of High Technologies, Taras Shevchenko National University of Kyiv, 64/13, Volodymyrska Street, 01601 Kyiv, Ukraine*

[d]*Institute of Macromolecular Chemistry, National Academy of Sciences of Ukraine, 48, Kharkivske shosse, 02160 Kyiv, Ukraine*

[e]*University of Colorado Colorado Springs, 420 Austin Bluffs, Parkway, CO, USA*

†Electronic supplementary information (ESI) available. See DOI: 10.1039/d1an02173g

enables the fluorimetric registration of various analytes with an attomolar limit of detection and single-molecule detection by exploiting the localized surface plasmon excitation in metal nanoparticles.[18–20]

PEF-based immunosensors were reported to detect different mycotoxins such as ochratoxin A, fumonisin B1, deoxynivalenol with the limits of detection in the ng kg^{-1} – μg kg^{-1} range.[21,22] For example, gold nanoparticles (AuNPs) were used as signal enhancers for fluorescence-based detection of aflatoxin B1, resulting in developing highly-sensitive immunosensor assay.[23] AuNPs were obtained using green synthesis and further conjugated with anti-AFB1 antibodies. Thus enhancement of the sensitivity of the immunosensors for aflatoxin B1 detection was demonstrated.[23] PEF technique in different implementations for enhanced sensitivity of fluorescent immunosensor detection of aflatoxins was reported for reaching the limits of detection down to 50 fg mL^{-1}.[23–26]

Moreover, emerging applications of molecularly imprinted polymers (MIPs) as artificial receptors in sensors based on plasmon- and surface-enhanced spectroscopies were reported.[27,28] PEF-based sensor exploiting core–shell Ag@SiO$_2$ hybrid nanostructures and boronate MIP was demonstrated for sensitive detection and specific recognition of riboflavin in human urine with the limit of detection of 3.3 ng mL^{-1}.[28] Silica shell of the thickness 15 nm has been used a spacer on the surface of Ag nanoparticles with an average diameter of 60 nm to produce the fluorescence enhancement factor of 27.6. The sensor exhibited a linear relationship between the fluorescence intensity and riboflavin concentration in the range 10–700 ng mL^{-1}, imprinting efficiency of 51%, and fast reaching binding - equilibrium within 20 min. Several MIP-plasmonic sensors based on surface-enhanced Raman scattering (SERS) readout were developed recently,[29–31] confirming the possibility of combining the plasmonic enhancement technique with MIP technology for the selective detection of various analytes. The difference of signal enhancement mechanisms in MIP-plasmonic sensors using PEF and SERS phenomena was reported, implying more complex nature of enhancement factor in PEF as a compromise between the electric field enhancement and fluorescence quenching.[28]

To achieve the highest fluorescence enhancement factor, - the PEF approach - usually requires precise control and complex lithographic techniques to tune the plasmonic nanoparticles into a spectral-spatial configuration with the fluorophore and provide the largest plasmonic "hot spots" intensity while keeping the fluorescence quenching low.[18–20] At the same time, relatively simple and tunable in situ syntheses of plasmonic nanoparticles inside MIPs were demonstrated by chemical or photoreduction methods.[32–35] Importantly, these fabrication techniques allow optimization of the plasmonic enhancement of the intramolecular optical processes, e.g., in SERS spectroscopy[34] by changing the concentration of the precursor, which defines the size and concentration of the synthesized nanoparticles as well as molecule-nanoparticle distance.

MIP films or thin films with incorporated metal nanoparticles can serve as an alternative to natural antibodies and receptors for producing sensing chips for the fluorescent affinity sensor. MIPs are generally as sensitive and selective as natural receptors, while they normally demonstrate superior stability and inexpensive, user-friendly production procedures. On the other hand, AgNPs can be used as an enhancer for AFB1 fluorescence detection and a sensor signal amplifier. Gold and silver nanoparticles can be formed during the in situ synthesis in the structure of a number of polymers, e.g., poly(ethyleneimine), poly(hydroxyethyl methacrylate), poly(vinylpyrrolidone), novolak, poly(4-vinylphenol), poly(4-vinylphenol)-co-(methyl methacrylate), poly(styrene-co-allyl alcohol),[36,37] and MIPs.[38,39] The size and shape of the described nanoparticles as well as the distance between them, which are the important parameters determining their ability to enhance fluorescence intensity, can be controlled.[36,37]

This paper introduces the novel nanostructured composite polymeric films with embedded in situ-synthesized Ag nanoparticles and a portable sensor device prototype for the PEF-based MIP-assisted detection of aflatoxins. We describe the fabrication protocol of MIP films and their sensing performance in terms of concentration-dependent response, selectivity, and optimization of Ag nanoparticles content. To the best of our knowledge, the proposed in situ synthesis route of the sensor films by simultaneous UV photoreduction of Ag nanoparticles and UV polymerization of the monomer- mixture was used here for the first time for the fluorescent detection of aflatoxins. We hypothesize that the metal-enhanced fluorescence significantly increases AFB1 quantum yield and brightness and, consequently, improves the AFB1 detection limit. The proposed prototype of portable sensor system can be used for rapid and reliable aflatoxin B1 monitoring at extremely low concentration levels.

2. Experimental

2.1. Materials

Aflatoxin B1 (AFB1), aflatoxin G2 (AFG2), AgNO$_3$, ochratoxin A (OTA), acrylamide (AA), dimethylformamide (DMF), polyethyleneglycol M_w 20 000 (PEG 20 000), triethyleneglycoldimethacrylate (TGDMA) were purchased from Sigma-Aldrich (St Louis, USA). Oligourethaneacrylate (OUA) was synthesized as described in,[40] DMF was distilled under reduced pressure over CaO and P$_2$O$_5$, γ-methacryloxypropyltrimethoxysilane was purchased from Serva (Heidelberg, Germany). Microscope glass slides 25.4 × 76.2 mm, 1 mm-thick (Marienfeld, Germany) were cut to 13 × 25.4 mm pieces prior to MIP films' immobilization. All the other reagents of analytical grade were purchased from Sigma-Aldrich (USA), UkrOrgSyntez (Ukraine), and Macrochim (Ukraine) and used without additional purification. The samples naturally contaminated with aflatoxin AFB1 and characterized by traditional analytical methods (HPLC and ELISA) were obtained from Romer Labs (Kyiv, Ukraine).

2.2. Immobilization of MIP films on the glass surfaces

The aflatoxin B1-selective MIP films were synthesized on the surface of glass slides treated with γ-methacryloxypropyltrimethoxysilane to

provide covalent immobilization of the MIP thin film on the glass surface. The monomer mixture (Table 1) was polymerized between two glass slides, one of which was treated with γ-methacryloxypropyltrimethoxysilane.

The monomer mixtures were heated at 80 °C for 2 min to dissolve PEG 20 000. This was followed by the addition of the initiator and a final 30 min-polymerization step initiated by UV light (λ = 365 nm, intensity 3.4 W m^{-2}).

To obtain AFB1-selective MIP films with AgNPs embedded in their structure, 0.6–291 mM AgNO$_3$ were added to the initial monomer mixtures used for the synthesis of AFB1-selective films. AgNPs were formed *in situ* during the pre-heating step and further UV-initiated polymerization procedure.

The MIP films were synthesized using a dummy template-based approach with ethyl-2-oxocyclopentanecarboxylate as a template molecule and acrylamide as a functional monomer.[41] The corresponding non-imprinted polymer (NIP) films were obtained without ethyl-2-oxocyclopentanecarboxylate so that no aflatoxin B1-selective sites were formed in their structure. The polymerization was followed by an 8 h Soxhlet extraction procedure in ethanol to remove the dummy template and the other monomers, which were not included in the structure of the MIP and NIP films. That was followed by the other 8 h extraction procedure in distilled water at 80 °C to remove PEG 20 000 responsible for the pore formation in the polymers. Finally, the fully-formed MIP and NIP films immobilized on the glass slides were dried and stored at room temperature for further investigations. The thickness of the MIP films immobilized on glass surfaces was estimated using Electronic Digital Caliper 0–300 micrometer ("Adoric", Ningbo, China).

2.3. On-chip fluorescent sensor for the selective detection of AFB1

The detection of aflatoxin B1 is based on its natural ability to fluorescence. The fluorescence sensor signals were excited with UV-irradiation (λ = 365 nm) after 30 min incubation of both MIP and NIP sensor chips in 0.1–500 ng mL^{-1} AFB1 in 20 mM Na-phosphate buffer pH 6.0, containing 10% acetonitrile. Blue fluorescence of AFB1 selectively adsorbed on the surface of glass chips coated with thin MIP films was registered with a standard laboratory spectrofluorimeter Fluoromax_ PLUS_PR928P (Horiba, Japan).

After incubation, the MIP and NIP films were rinsed in 20 mM Na-phosphate buffer pH 6.0, containing 10% aceto-

nitrile, and dried at room temperature. The sensor responses were registered after UV-irradiation of the sensor chips (MIP films covalently attached to the surface of glass slides) fixed in a solid samples' holder of the spectrofluorimeter (Ex bandwidth 5 nm, Em bandwidth 2.5 nm, excitation wavelength 365 nm, measurement range 395–550 nm, and emission wavelength 420 nm) directly at the films' surface (Fig. S4†).

2.4. Portable fluorimeter for aflatoxin B1 detection in in-field conditions

Fluorescence measurements were performed using the Fluoromax_PLUS_PR928P (Horiba, Japan) as described in section 2.3. A home-built portable fluorimeter was also used for the fluorescence measurements with the optical signal in the vicinity of the wavelength of aflatoxin fluorescence (365–400 nm). The optical scheme of the device is shown in Fig. 1.
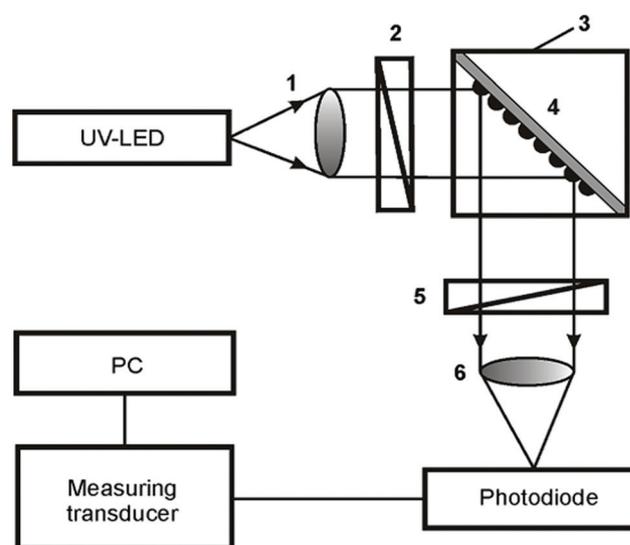
The portable fluorimeter uses ultraviolet (365 nm) LED as an excitation light focused by a collimator (Ocean Insight 74-UV) and sent through an optical cable to the sample holder with a built-in bandpass filter (365 nm). The sensor chips were fixed by a specially designed holder for solid samples. The fluorescent signal amplified by the plasmonic nanochip is collected by a collimator and is registered with a photodiode through a longpass filter (400 nm). The recorded signal is transmitted *via* Bluetooth to the receiving gadget or, after focusing, with an optical cable to the spectrometer and computer.

2.5. TEM for synthesized AgNPs in MIP film structure

Transmission electron microscopy (TEM) was carried out to study the morphology and size distribution of AgNPs in the MIP films. Since the reduction of the silver ions was used to

Fig. 1 Optical setup of portable fluorimeter: 1, 6 – collimators, 2 – bandpass filter (365 nm), 3 – sample holder, 4 – nanochip with highly-conductive nanoparticles, 5 – longpass filter (400 nm).

Table 1 Compositions of the monomer mixture for the MIP and NIP films' synthesis

Monomer/oligomer	MIP	NIP
Ethyl-2-oxocyclopentanecarboxylate	10 mg	—
Acrylamide	9 mg	9 mg
TGDMA	162 mg	162 mg
OUA	29 mg	29 mg
DMF	100 μL	100 μL
Polyethyleneglycol (M_w 20 000)	30 mg	30 mg
2,2′-Dimethoxy-2-phenylacetone	0.2 mg	0.2 mg

synthesize AgNPs, the preparation of samples for TEM imaging was performed using the same polymerization protocol on a surface of a copper grid. The monomer mixture containing 10 mg ethyl-2-oxocyclopentanecarboxylate, 9 mg acrylamide, 162 mg TGDMA; 29 mg OUA, 100 μL DMF, 30 mg polyethyleneglycol M_w 20 000, 0.2 mg 2,2′-dimethoxy-2-phenylacetone and 1.5 mM $AgNO_3$ was used for the polymerization. The polymer was formed on the surface of the copper grid 3 mm diameter. The copper grid was placed on a glass slide (13 × 25.4 mm size) surface. Then, 0.5 μL of the monomer mixture was dropped onto the grid, and another glass slide was placed over the sample. The monomer mixtures were polymerized between two glass slides kept with two binder clips (18 mm size). The polymerization was initiated using UV light (λ = 365 nm, intensity 3.4 W m^{-2}) and performed for 30 min. Finally, the MIPs synthesized on the copper grid surface were used for TEM investigations. Transmission electron microscope (JEM-1230, JEOL, Japan) with an accelerating voltage of 50–120 kV was used to investigate AgNPs formed in the MIP film structure.

3. Results and discussion

The functional monomer capable of effective recognition of aflatoxin B1 was chosen based on our previous results,[41] which demonstrated acrylamide as the most effective monomer for selective binding. The covalent immobilization procedure for the acrylamide-containing MIP thin film on the surface of the glass slides based on the application of γ-methacryloxypropyltrimethoxysilane was developed and optimized (section 2.2).

The registration principle of the proposed MIP-AgNPs sensor film is based on the selective binding of aflatoxin B1 in analyzed samples by nanoreceptor sites and registration of the plasmon-enhanced fluorescence signal of aflatoxin molecules excited by UV irradiation. A home-built portable fluorimeter registered the fluorescent sensor signals. Silver nanoparticles in the MIP films' structure amplify the fluorescence signal due to the enhanced local electric field resulting from localized surface plasmon resonance excitation in nanoparticles.

The developed sensor chips based on immobilized acrylamide-containing MIP thin films were produced and tested for their ability to generate fluorescent sensor responses due to AFB1 binding. NIP films were obtained using the same compositions of monomers except for the dummy template (ethyl-2-oxoceclopentanecarboxylate)[41] that was added to the MIP compositions only. The thickness of the MIP films immobilized on glass surfaces was estimated as 80 μm. The aflatoxin B1 detection is possible due to its natural ability to fluorescence. The sensor signals were excited with UV-irradiation (λ = 365 nm) after incubation of the developed sensor chips in 15–500 ng mL^{-1} solutions of AFB1, while blue fluorescence of the toxin of interest selectively adsorbed on the surface of the chips was registered at λ = 420 nm directly at the sensor chip surface with both the standard laboratory spectrofluorimeter and the

home-built portable fluorimeter for AFB1 in-field detection (section 2.4).

Fig. 2 shows a typical calibration plot for the fluorescent sensor systems based on acrylamide-containing MIP films immobilized on the surface of a glass chip. Fig. 2a graph demonstrated a typical form indicating the presence of affinity receptor sites for AFB1 binding in MIP film's structure in contradistinction to the NIP film, where the calibration plot is linear. As seen for MIP at high concentrations, receptor binding sites are saturated.

The limits of detection were determined based on European standard ISO 11843-2:2000.[42] The lowest detection limit (LOD) for AFB1 detection was estimated to be 10 ng mL^{-1}, while the linear dynamic range was 10–250 ng mL^{-1}
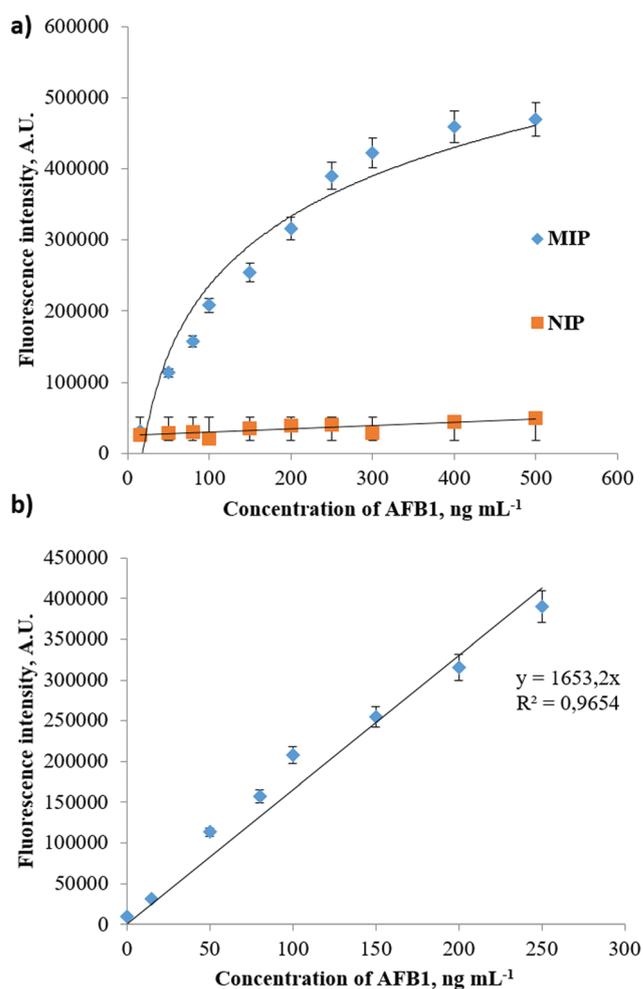

Fig. 2 Typical calibration curves of the MIP-based fluorescent sensor system for AFB1 detection: a – fluorescence of $AgNO_3$-free thin films immobilized on the glass surfaces was registered after incubation in 5–500 ng mL^{-1} AFB1 solutions; b – the linear part of the calibration plot of the fluorescent sensor system obtained after incubation of the sensor chips in 5–250 ng mL^{-1} solutions of AFB1. The measurements were performed in 20 mM Na-phosphate buffer pH 6.0, containing 10% acetonitrile. Spectrofluorimeter Fluoromax_PLUS_PR928P (λ_{ex} = 365 nm, λ_{em} = 420 nm) was used for the measurements.

(Fig. 2b). The storage stability for the sensing chips for AFB1 fluorescent detection was assessed for 18 months at room temperature.

The sensor described in this paper has a better LOD (10 ng mL^{-1}) as compared to the previously-reported sensor based on the application of 60 μm-thick free-standing MIP films[41] whose LOD was 15 ng mL^{-1}, as well as better reproducibility (R = 107% *vs. R* = 87%). Moreover, the proposed sensor chips are also characterized by superior mechanical stability.

The ability of the developed fluorescent sensors based on MIP-based sensor chips to discriminate between the toxin of interest and its potential interferents that are often present in the extracts of the analyzed cereal samples was investigated using the other structurally similar fluorescent mycotoxins, *i.e.*, aflatoxins B2 and G2 (AFB2, AFG2) as well as ochratoxin A (OhA).

The differential fluorescent sensor signals, generated with the immobilized MIP-based sensor chips in response to the addition 100 ng mL^{-1} AFB1, AFB2, AFG2, and OhA, were evaluated (Fig. 3).

Fig. 3 exemplifies that the MIP films immobilized on the glass surface exhibit preferential binding of the toxin of interest as compared to the potentially interfering fluorescent substances. However, the achieved LOD for AFB1 detection (10 ng mL^{-1}) required further improvement to ensure sensitive detection of the target toxin in food and feeding stuffs. Therefore, the initial MIP composition was further modified by incorporating Ag nanoparticles in their structure.

Here we demonstrate the *in situ* formation of Ag nanoparticles directly in the MIP thin film during polymer formation. Silver nanoparticles (AgNPs) were synthesized using a reduction of silver nitrate (AgNO$_3$) added to the initial composition for the imprinted polymer synthesis in specific concentrations. The proposed synthetic route is based on silver nanoparticles synthesis in MIP thin film structure due to AgNO$_3$ reduction during the pre-heating step of the initial monomer mixture used for the MIP formation followed by UV-initiated photopolymerization. To the best of our knowledge, this is the first demonstration of Ag nanoparticles synthesis in the MIP structure for the effective fluorescent detection of aflatoxins. AgNO$_3$ was added to the initial monomer mixture to the final concentrations varying from 0.6 mM to 291 mM.

The morphology of the AgNPs formed in the structure of the AFB1-selective MIP films was investigated using TEM microscopy. Fig. 4 shows TEM images of the MIP thin films obtained by *in situ* polymerization with the AgNPs embedded in the polymer structure.

As one can see, the shape of AgNPs formed in the structure of the MIP films at the optimized conditions (from the monomer compositions containing 1.5 mM AgNO$_3$ in the initial mixture of monomers for the MIP synthesis) was close to spherical shape with the size of 30–70 nm. The nanoparticles were evenly distributed in the structure of the polymer. According to the numerical calculations of the system with spherical silver nanoparticles (Fig. S1 in ESI†), this size of AgNPs provided some fluorescence enhancement, and, at the same time, there is a possibility to improve the already reached enhancement results by increasing the nanoparticle size (Fig. S2 in ESI†). Some deviations from the spherical shape (*i.e.*, rectangular, hexagonal) were observed, as one can see in Fig. 4. This limits the results of the used model and the possibility of further size growth for spherical nanoparticles under the used polymerization conditions. We note that the presence of copper grid during polymerization procedure, which could influence the reduction of silver ions and, consequently, the morphology of synthesized nanostructures, should be considered.

The rule of plasmonic enhancement of fluorescence stating that the surface plasmon resonance bands are supposed to overlap with the excitation or emission bands of the fluorophore molecules[43–45] was confirmed in this work. Taking into account that the measured LSPR wavelength position of the prepared Ag nanoparticles was about 407 nm, the LSPR band of spherical AgNPs overlaps significantly with the excitation and emission bands of aflatoxin B1 exhibiting peaks at 365 nm (ref. 41) and 420 nm, respectively (Fig. S3†), which satisfies a condition of plasmon resonance energy transfer between the nanoparticle and the fluorophore. Moreover, due to the proposed AgNO$_3$ reduction by the initial monomer mixture, the prepared Ag nanoparticles are mainly surrounded by the polymer that creates an advantageous condition for the mechanism of fluorescence enhancement in comparison with possible fluorescence quenching.

All the MIP and NIP Ag-containing polymers immobilized on the surface of glass slides were used as sensor chips for aflatoxin B1 detection. The ability of AgNPs formed in the polymer structure to improve the detection limit of the target mycotoxin due to the plasmon-enhanced fluorescence phenomenon was investigated. All synthesized films were
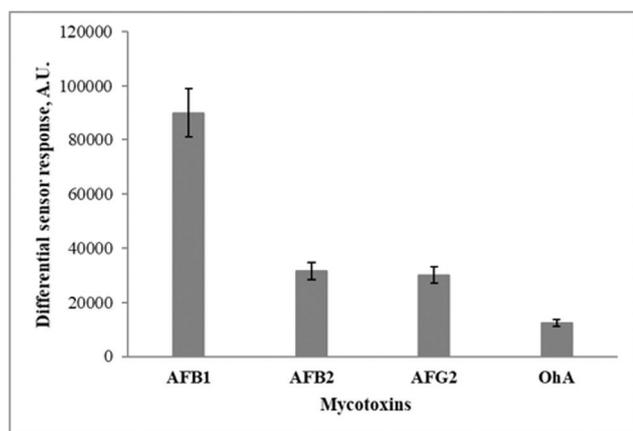
Fig. 3 Cross-selectivity of differential sensor responses* of the fluorescent sensor system based on AFB1-selective MIP thin films immobilized on glass slides' surface. Differential sensor responses after the addition of 100 ng mL^{-1} AFB1, AFG2, and OTA were estimated. The measurements were performed in 20 mM Na-phosphate buffer pH 6.0, containing 10% acetonitrile. *Differential sensor responses were calculated as differences between sensor responses generated by the MIP and NIP thin polymeric films immobilized on the surface of glass slides.
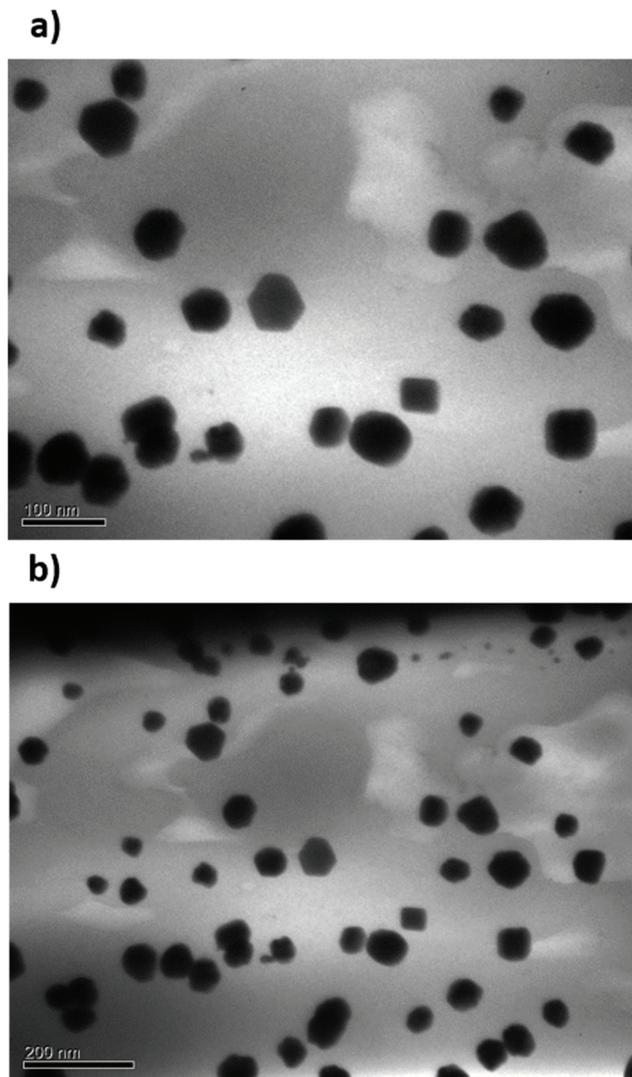
Fig. 4 TEM images of AgNPs formed in the structure of MIP thin polymer films synthesized with AA as a functional monomer taken at different magnifications (scale 100 nm (a) and 200 nm (b)).

Fig. 5 Fluorescent sensor responses of the sensors based on AgNPs-containing MIP thin films synthesized with different $AgNO_3$ concentrations in response to the addition of 100 ng mL^{-1} AFB1. The measurements were performed in 20 mM Na-phosphate buffer pH 6.0, containing 10% acetonitrile.

tested for their ability to bind AFB1 from aqueous solutions and generate the fluorescent sensor response, as shown in Fig. 5.

For the MIP films synthesized from the mixtures containing 1.5 mM $AgNO_3$, a 14-fold increase in the value of the fluorescent sensor responses compared to the AgNPs-free MIP films due to AFB1 addition was observed Fig. 6. The higher and lower $AgNO_3$ concentrations added to the MIP composition resulted in significantly lower (2.1–4.5-fold) enhancement effects. Higher concentrations of silver nitrate had the opposite effect on AFB1 fluorescence. For MIP films synthesized from the mixtures containing above 15 mM $AgNO_3$, quenching of aflatoxin B1 fluorescence was observed.

Fig. 6 shows the enhancement of the fluorescence intensity of aflatoxin B1 due to the surface plasmon resonance in AgNPs. All measurements were carried out using
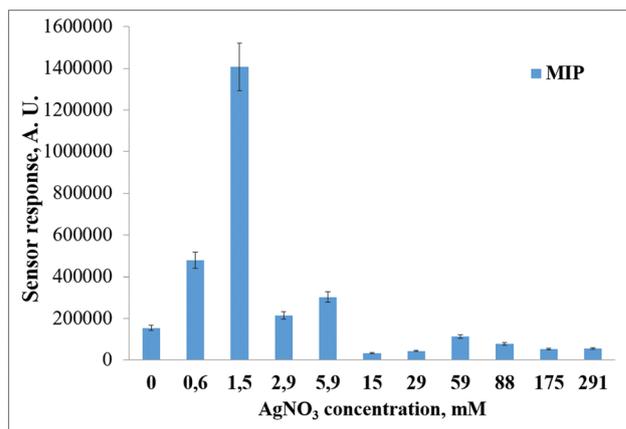
Fluoromax_PLUS_PR928P spectrofluorimeter, as well as portable fluorimeter (excitation wavelength 365 nm, measurement range 395–550 nm). According to these results, the fluorescence spectra obtained using standard laboratory spectrofluorimeter Fluoromax_PLUS_PR928P (Horiba, Japan) and portable fluorimeter were identical.

The addition of $AgNO_3$ to the initial composition of monomers leading to the formation of Ag nanoparticles in the polymer structure results in a significant increase in values of the sensor responses and a significant increase of the aflatoxin B1-selective MIP films' imprinting factor. We observed a 4.7-fold increase in the imprinting factor at 100 ng mL^{-1} AFB1 concentration.

The AgNP-containing MIP-based sensor chips were tested as selective elements of the fluorescent sensor, and the ability of AgNPs to improve the minimal detection limit of aflatoxin B1 detection was studied. Typical calibration plots for the fluorescent sensor systems based on acrylamide-containing MIP-films synthesized with addition 1.5 mM $AgNO_3$ are presented in Fig. 7.

The minimal detection limit of the aflatoxin B1-selective sensor system decreased by a factor of 33 because of the plasmon-enhanced fluorescence: the LOD was decreased down to 0.3 ng mL^{-1} for AgNPs-based MIP films as compared to 10 ng mL^{-1} for the unmodified MIP-based sensor systems.

The linear dynamic range of the fluorescent sensor is 0.3–25 ng mL^{-1}, as can be seen in Fig. 7 (see Fig. S5† for low AFB1 concentrations).

The fluorescent sensor intensity signals of the sensors based on AgNPs-containing MIP films were 40–80% higher than those of AgNPs-free MIPs, as shown in Fig. 8.

AgNPs-containing MIP thin films demonstrate superior properties as sensitive elements of a portable fluorescent sensor system as compared to unmodified MIPs. They can generate significantly higher sensor responses, which resulted in the 33-fold decrease of the minimal detection limit for AFB1.
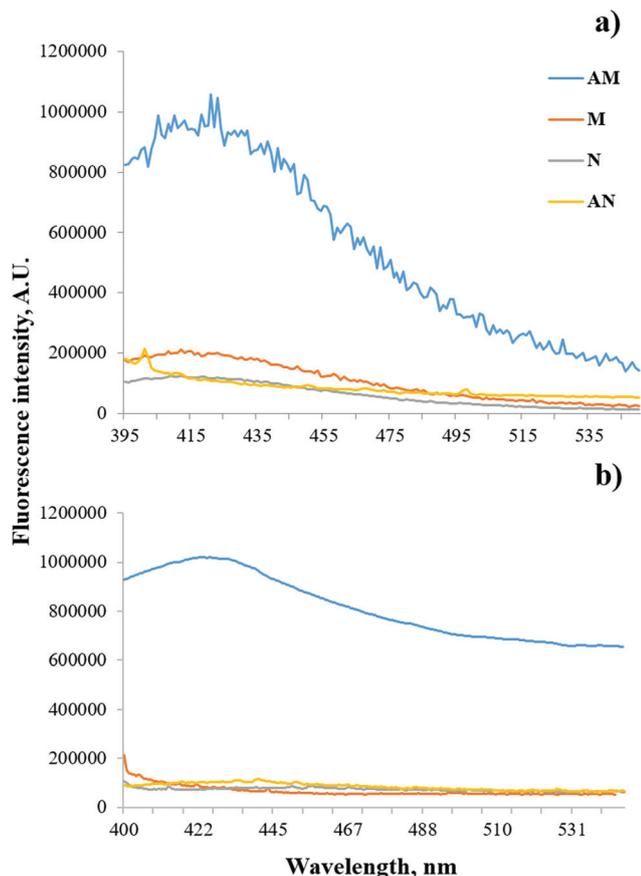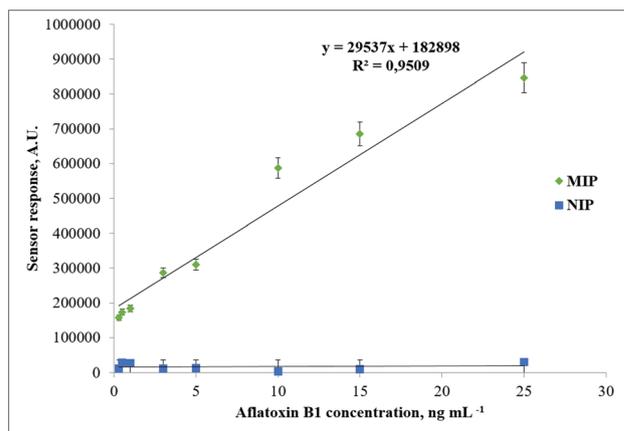
Fig. 6 Fluorescence spectra of aflatoxin-B1-sensitive and NIP films obtained with and without AgNO₃ in the initial mixture of monomers for the film synthesis (100 ng mL⁻¹ AFB1 were added to the analyzed sample): AM – MIP film obtained from the monomer mixture containing 1.5 mM AgNO₃; M – MIP film obtained from the monomer mixture without AgNO₃; N – NIP film obtained from the monomer mixture without AgNO₃; AN – MIP film obtained from the monomer mixture containing 1.5 mM AgNO₃. Fluoromax_PLUS_PR928P spectrofluori-meter (a) and portable fluorimeter (b) (λ_{ex} = 365 nm, λ_{em} = 420 nm) were used for the measurements.

Fig. 7 Typical calibration plots of the AgNPs-containing MIP-film-based fluorescent sensor systems for AFB1 detection. Fluorescence of AgNPs-containing MIP and NIP thin polymeric films immobilized on the glass slides synthesized with AA as a functional monomer with the addition of 1.5 mM AgNO₃. The measurements were performed in 20 mM Na-phosphate buffer pH 6.0, containing 10% acetonitrile. Portable fluorimeter (λ_{ex} = 365 nm, λ_{em} = 420 nm) was used for the measurements.
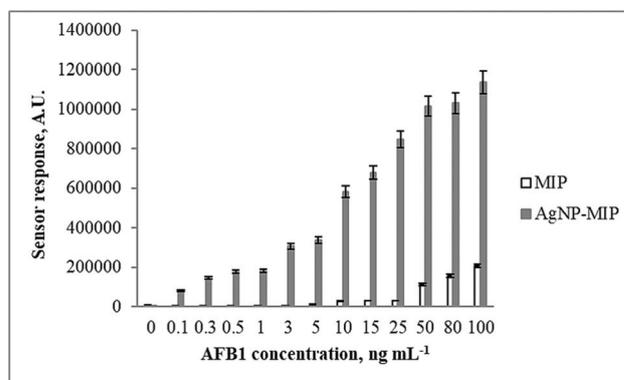
Fig. 8 Comparison of fluorescent sensor responses values obtained from the sensors based on AgNPs-containing and AgNPs-free MIP chips after adding 0.1–100 ng mL⁻¹ AFB1. AgNPs-containing MIP thin films were synthesized using AA as a functional monomer with the addition of 1.5 mM AgNO₃. The measurements were performed in 20 mM Na-phosphate buffer pH 6.0, containing 10% acetonitrile. Spectrofluorimeter Fluoromax_PLUS_PR928P (λ_{ex} = 365 nm, λ_{em} = 420 nm) was used for the measurements.

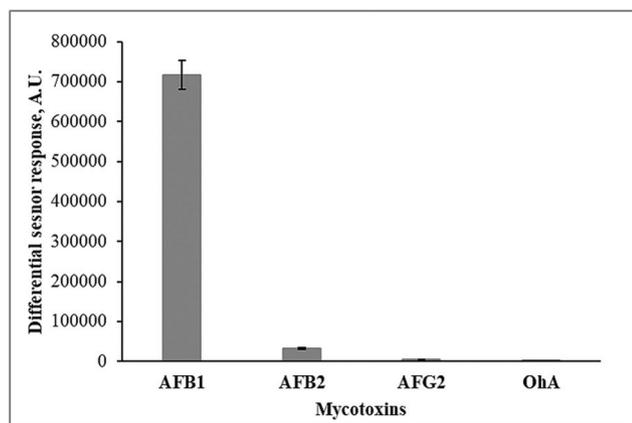The selectivity of the newly synthesized AgNPs-containing sensor chips was also evaluated (Fig. 9).

The differential fluorescent sensor signals, generated with the AgNPs-containing MIP sensor chips in response to the addition of 15 ng mL⁻¹ AFB1, AFB2, AFG2, and OTA, were evaluated.

The developed sensor system based on AgNPs-containing MIP sensor chips exhibits better selectivity. The sensor responses initiated by the addition of the potentially interfering AFB1 structural analogues (AFB2, AFG2, and OhA) were negligible compared to those generated by the target myco-toxin (AFB1). Moreover, the selectivity of the AgNPs-containing MIP-based sensors was much better than the selectivity of the unmodified MIP films shown in Fig. 3.

In order to evaluate the performance of the developed portable fluorescent sensor system based on AgNPs-containing MIP sensor chips for the food quality monitoring, the real

cereal samples were tested for AFB1 contamination using the developed method. Five different maize flour samples were tested. The first three samples (sample no. 1, 2, and 3) were naturally contaminated with AFB1 and provided by Romer Labs (Kyiv, Ukraine): sample no. 1 – "Romer Labs CheckSample Survey Aflatoxins in corn (CSSMY013 – M17411A)"; sample no. 2 – "Quality control material Aflatoxins in corn, low level", sample no. 3 – "Quality control material Aflatoxins in corn, mid-level". The manufacturer characterized all the naturally contaminated samples for the AFB1 content by standard analytical methods (HPLC and ELISA). Also, AFB1-

Fig. 9 Cross-selectivity of the fluorescent sensor* based on AgNPs-containing MIP thin films synthesized with 1.5 mM AgNO₃ and AA as a functional monomer. Differential sensor responses were registered after the addition of 15 ng mL^{-1} AFB1, AFB2, AFG2, and OTA. The measurements were performed in 20 mM Na-phosphate buffer pH 6.0, containing 10% acetonitrile. Spectrofluorimeter Fluoromax_PLUS_PR928P (λ_{ex} = 365 nm, λ_{em} = 420 nm) was used for the measurements. *Differential sensor responses were calculated as differences between sensor responses generated by the fluorescent sensors based on MIP and NIP thin polymeric films.

free maize flour samples produced by two different manufacturers ("Lavka Tradytsiy", Ukraine (sample no. 4), "Dobrodiya Foods", Kyiv, Ukraine (sample no. 5)) and purchased in the local supermarket were used in the investigation. According to the standard procedure described earlier, the procedure of AFB1 extraction from maize flour was made using 80 : 20 v/v acetonitrile : H$_2$O solution.[41,46] The AFB1-free flour extracts were spiked with 1 (sample no. 4) and 5 (sample no. 5) ng mL^{-1} AFB1. Results of aflatoxin B1 detection in real maize flour samples using the fluorescent sensor system based on AgNPs-containing AFB1-selective MIP thin films are presented in Table 2. Fluorescent sensor responses were estimated by the home-built portable fluorimeter.

The results presented in Table 2 clearly demonstrate the efficiency of the proposed AgNPs-containing MIP-based sensor system for monitoring AFB1 contamination of the cereal

Table 2 Detection of AFB1 in maize samples by the portable fluorescent AgNPs-containing MIP-based sensor system and traditional analytical methods

Sample No.	Amount of AFB1 in the sample (according to the traditional method)	Amount of AFB1 in the sample (according to portable fluorescent MIP-based sensor system)	Recovery (R, %)
1	7 µg kg^{-1}	6.4 ± 3.2 µg kg^{-1}	109
2	4.2 ± 1.7 µg kg^{-1}	4.5 ± 2.0 µg kg^{-1}	93
3	7.3 ± 2.9 µg kg^{-1}	7.7 ± 0.9 µg kg^{-1}	94
4	1 ng mL^{-1}	1.9 ± 0.9 ng mL^{-1} (0.8 µg kg^{-1})	90
5	5 ng mL^{-1}	5.4 ± 0.8 ng mL^{-1} (2 µg kg^{-1})	93

samples. The obtained results of the analytical identification of aflatoxins corresponded to the traditional instrumental and immunochemical methods.

4. Conclusions

A portable fluorescent sensor system based on AgNPs-containing MIP films capable of selective aflatoxin B1 recognition suitable for in-field application was developed and demonstrated. AgNPs were synthesized *in situ* directly in the structure of the MIP films during the polymerization procedure. This approach resulted in a 33-fold decrease in the detection limit and a significant increase in the overall value of the sensor responses due to the LSPR phenomenon compared to the sensors based on AgNPs-free MIP sensor chips. The minimal detection limit for AFB1 was estimated as 0.3 ng mL^{-1}, the linear dynamic range of the developed fluorescent sensor was 0.3–25 ng mL^{-1}. Negligible binding of interferents that can be potentially present in analyzed cereal extracts was observed for the aflatoxin B1-selective AgNPs-containing MIP sensor chips. The formation of 30–70 nm diameter AgNPs in the structure of the MIP films evenly distributed in the polymer was confirmed by TEM studies. The developed sensor system was effective for the aflatoxin B1 analysis in both spiked and naturally contaminated samples of cereal extracts.

Author contributions

T. Sergeyeva: Conceptualization, methodology, writing – original draft preparation, project administration. D. Yarynka: Investigation – synthesis of silver nanoparticle – containing MIP membranes and estimation of their sensor properties, TEM studies, writing – original draft preparation. V. Lytvyn: Investigation – development of a portable fluorimeter. P. Demydov: Investigation – development of a portable fluorimeter. A. Lopatynskyi: Investigation – development of a portable fluorimeter, modeling, writing – original draft preparation, Ye. Stepanenko: Investigation – fluorescence measurements, O. Brovko: Investigation – synthesis of oligourethaneacrylate, A. Pinchuk: Conceptualization, writing – reviewing and editing, V. Chegel: Conceptualization, methodology, investigation – TEM studies, modeling, writing – original draft preparation, project administration.

Conflicts of interest

There are no conflicts to declare.

Acknowledgements

structured polymeric films") is gratefully acknowledged. Any opinions, findings, conclusions, or recommendations expressed in this material are those of the author(s) and do not necessarily reflect the views of CRDF Global.

References

1 N. J. Mitchell, E. Bowers, C. Hurburgh and F. Wu, *Food Addit. Contam., Part A*, 2016, **33**, 540–550.

2 W. E. O. Campos, L. B. Rosas, A. P. Neto, R. A. Mello and A. A. Vasconcelos, *J. Food Compos. Anal.*, 2017, **60**, 90–96.

3 M. Ivešić, Z. Kuharić, Z. Pavlek, Z. Jakopović, I. Čanak, J. Frece, K. Markov and J. Bošnir, *Toxicol. Lett.*, 2018, **295**, S147–S148.

4 S. Zhan, J. Hu, Y. Li, X. Huang and Y. Xiong, *Food Chem.*, 2021, **342**, 128327.

5 J. Wu, L. Zeng, N. Li, C. Liu and J. Chen, *Food Chem.*, 2019, **298**, 125034.

6 M. Mousivand, L. Anfossi, K. Bagherzadeh, N. Barbero, A. Mirzadi-Gohari and M. Javan-Nikkhah, *Anal. Chim. Acta*, 2020, **1105**, 178–186.

7 L. Tang, Y. Huang, C. Lin, B. Qiu, L. Guo, F. Luo and Z. Lin, *Talanta*, 2020, **214**, 120862.

8 A. Sharma, R. Khan, G. Catanante, T. A. Sherazi, S. Bhand, A. Hayat and J. L. Marty, *Toxins*, 2018, **10**, 197.

9 F. Tam, G. P. Goodrich, B. R. Johnson and N. J. Halas, *Nano Lett.*, 2007, **7**, 496–501.

10 T. Ribeiro, C. Baleizão and J. P. S. Farinha, *Sci. Rep.*, 2017, **7**, 1–12.

11 M. Li, S. K. Cushing and N. Wu, *Analyst*, 2015, **140**, 386–406.

12 V. A. Zenin, A. Andryieuski, R. Malureanu, I. P. Radko, V. S. Volkov, D. K. Gramotnev, A. v. Lavrinenko and S. I. Bozhevolnyi, *Nano Lett.*, 2015, **15**, 8148–8154.

13 Y. Wu, M. R. K. Ali, K. Chen, N. Fang and M. A. El-Sayed, *Nano Today*, 2019, **24**, 120–140.

14 Y. Jeong, Y.-M. Kook, K. Lee and W.-G. Koh, *Biosens. Bioelectron.*, 2018, **111**, 102–116.

15 A. Govorov, P. L. H. Martínez and H. V. Demir, *Understanding and Modeling Förstertype Resonance Energy Transfer (FRET): Introduction to FRET*, Springer, 2016, vol. 1.

16 J.-F. Li, C.-Y. Li and R. F. Aroca, *Chem. Soc. Rev.*, 2017, **46**, 3962–3979.

17 N. Fontaine, A. Picard-Lafond, J. Asselin and D. Boudreau, *Analyst*, 2020, **145**, 5965–5980.

18 L. Zhou, F. Ding, H. Chen, W. Ding, W. Zhang and S. Y. Chou, *Anal. Chem.*, 2012, **84**, 4489–4495.

19 H. Cang, A. Labno, C. Lu, X. Yin, M. Liu, C. Gladden, Y. Liu and X. Zhang, *Nature*, 2011, **469**, 385–388.

20 A. Kinkhabwala, Z. Yu, S. Fan, Y. Avlasevich, K. Müllen and W. E. Moerner, *Nat. Photonics*, 2009, **3**, 654–657.

21 F. Todescato, A. Antognoli, A. Meneghello, E. Cretaio, R. Signorini and R. Bozio, *Biosens. Bioelectron.*, 2014, **57**, 125–132.

22 G. Koukouvinos, C.-E. Karachaliou, A. Kanioura, K. Tsougeni, E. Livaniou, S. E. Kakabakos and P. S. Petrou, *Processes*, 2021, **9**, 392.

23 K. S. Abhijith and M. S. Thakur, *Anal. Methods*, 2012, **4**, 4250–4256.

24 Y. Wang, J. Dostálek and W. Knoll, *Biosens. Bioelectron.*, 2009, **24**, 2264–2267.

25 K. S. Abhijith, K. v. Ragavan and M. S. Thakur, *Anal. Methods*, 2013, **5**, 4838–4845.

26 X. Lv, Y. Li, W. Cao, T. Yan, Y. Li, B. Du and Q. Wei, *Sens. Actuators, B*, 2014, **202**, 53–59.

27 P. Liu, M. Guo, C. Lan, B. Huang, S. Yang, Y. Qiu and Y. Ma, *Mater. Express*, 2018, **8**(3), 272–278.

28 H. He, P. Muhammad, Z. Guo, Q. Peng, H. Lu and Z. Liu, *Biosens. Bioelectron.*, 2019, **146**, 111733.

29 R. Xing, Y. Wen, Y. Dong, Y. Wang, Q. Zhang and Z. Liu, *Anal. Chem.*, 2019, **91**, 9993–10000.

30 H. Li, Y. Wang, Y. Li, J. Zhang, Y. Qiao, Q. Wang and G. Che, *J. Phys. Chem. Solids*, 2020, **138**, 109254.

31 J. Feng, Y. Hu, E. Grant and X. Lu, *Food Chem.*, 2018, **239**, 816–822.

32 C. Deng, Y. Zhong, Y. He, Y. Ge and G. Song, *Microchim. Acta*, 2016, **183**, 431–439.

33 R. Hu, R. Tang, J. Xu and F. Lu, *Anal. Chim. Acta*, 2018, **1034**, 176–183.

34 Z. Wang, R. Yan, S. Liao, Y. Miao, B. Zhang, F. Wang and H. Yang, *Appl. Surf. Sci.*, 2018, **457**, 323–331.

35 P. Liu, R. Liu, G. Guan, C. Jiang, S. Wang and Z. Zhang, *Analyst*, 2011, **136**, 4152–4158.

36 R. Abargues, K. Abderrafi, E. Pedrueza, R. Gradess, J. Marqués-Hueso, J. L. Valdés and J. Martínez-Pastor, *New J. Chem.*, 2009, **33**, 1720–1725.

37 R. Abargues, J. Marques-Hueso, J. Canet-Ferrer, E. Pedrueza, J. L. Valdes, E. Jimenez and J. Martinez-Pastor, *Nanotechnology*, 2008, **19**(35), 355308, DOI: 10.1088/0957-4484/19/35/355308.

38 E. Aznar-Gadea, P. J. Rodríguez-Canto, J. P. Martínez-Pastor, A. Lopatynskyi, V. Chegel and R. Abargues, *ACS Appl. Polym. Mater.*, 2021, **3**, 2960–2970.

39 M. Riskin, Y. Ben-Amram, R. Tel-Vered, V. Chegel, J. Almog and I. Willner, *Anal. Chem.*, 2011, **83**, 3082–3088.

40 Y. L. Spirin, Y. S. Lipatov, V. v. Magdinets, L. M. Sergeyeva, Y. Y. Kercha, T. T. Savchenko and L. N. Vilenskaya, *Polym. Sci. U.S.S.R.*, 1968, **10**, 2463–2470.

41 T. Sergeyeva, D. Yarynka, E. Piletska, R. Linnik, O. Zaporozhets, O. Brovko, S. Piletsky and A. El'skaya, *Talanta*, 2019, **201**, 204–210.

42 ISO, N. (2000). 11843-2 (2000) Capability of detection, Part 2: Methodology in the linear calibration case. *Standard, NF ISO*, 11843-2.

43 T. Förster, *Ann. Phys.*, 1948, **437**(1–2), 55–75.

44 J. R. Lakowicz, *Plasmonics*, 2006, **1**(1), 5–33.

45 K. Aslan, J. R. Lakowicz and C. D. Geddes, *J. Phys. Chem. B*, 2005, **109**(13), 6247–6251.

46 *Analysis of Food Constituents*, ed. J. L. Multon, W. J. Stadelman and B. A. Watkins, Wiley-VCH, New York, Chichester, 1996, pp. 380–402.